IEEE Access
Multidisciplinary | Rapid Review | Open Access Journal

Received 3 August 2022, accepted 27 August 2022, date of publication 5 September 2022, date of current version 15 September 2022.

Digital Object Identifier 10.1109/ACCESS.2022.3204029

RESEARCH ARTICLE

GlauNet: Glaucoma Diagnosis for OCTA Imaging Using a New CNN Architecture

ANITA MANASSAKORN[1,2], SUPATANA AUETHAVEKIAT[3], VERA SA-ING[4], SUNEE CHANSANGPETCH[1,2], KITIYA RATANAWONGPHAIBUL[1,2], NOPPHAWAN URAMPHORN[5], AND VISANEE TANTISEVI[1,2]

[1]Center of Excellence in Glaucoma, Faculty of Medicine, Chulalongkorn University, Bangkok 10330, Thailand
[2]King Chulalongkorn Memorial Hospital, The Thai Red Cross Society, Bangkok 10330, Thailand
[3]Department of Electrical Engineering, Faculty of Engineering, Chulalongkorn University, Bangkok 10330, Thailand
[4]Department of Computer Science, Faculty of Science, Srinakarinwirot University, Bangkok 10110, Thailand
[5]Department of Ophthalmology, Faculty of Medicine, Vajira Hospital, Navamindradhiraj University, Bangkok 10300, Thailand

Corresponding author: Supatana Auethavekiat (asupatana@yahoo.com)

ABSTRACT Glaucoma is a neurodegenerative disease that affects the optic nerve head and causes visual field defect. Current investigations focus on neural component which may overlook other important factors such as the vascular cause. The optical coherence tomography angiography (OCTA) imaging has been developed and provided quantitative parameters that showed good diagnostic accuracy to detect glaucoma. However, those parameters are based on image processing of observed clinical findings, therefore, some image information can be lost. Convolutional neural network has been successfully applied for automatic feature extraction and object classification. In this study, the glaucoma diagnosis network, namely GlauNet, has been proposed. GlauNet consists of two sections: the feature-extraction section and the classification section. The feature-extraction section has three convolutional layers. Each convolutional layer is followed by rectified linear unit and maximum pooling layer. The classification section contains five fully connected layers. GlauNet was trained with 258 glaucomatous and 439 non-glaucomatous eyes. The visualization of the feature-extraction section showed the highlight in the area of optic nerve head and retinal nerve fiber layer in the superotemporal and inferotemporal regions. It was then tested on 27 glaucomatous and 48 non-glaucomatous eyes. Its sensitivity and specificity were 88.9% with 89.6%, respectively. The area under receiver operating characteristic curve of GlauNet was 0.89. GlauNet was robust against the artifacts. Its sensitivity and specificity were still higher than 80% (82.4% and 80.3%, respectively) when tested on 88 poor-quality images.

INDEX TERMS Artificial intelligence, convolutional neural network, deep learning, glaucoma, optical coherence tomography angiography, retinal blood vessels.

I. INTRODUCTION

Glaucoma is a major visual disability disease that presents with irreversible progressive neurodegeneration. It is caused by multiple factors. The prevalence of glaucoma in the world was 3.54% in the year 2014 and there will be about 111.8 million glaucoma patients in the year by 2040. The majority of patients will be in Asia and Africa [1]. Most of the patients are still asymptomatic until the late stage of the disease, as a result, the prevalence of undiagnosed patients were between 53% and 88% around the world [2], [3], [4], [5], [6]. In addition, challenge in glaucoma diagnosis is based on anatomical variations among people. The current definition of glaucoma is based on evaluation of neural structure of the optic nerve head and surrounding retina and visual field, while intraocular pressure is a major risk factor.

The mainstay glaucoma diagnostic tools in current practice are optic disc examination, optical coherence tomography (OCT) and visual field or perimetry. Optic nerve head assessment is the most commonly used method, because it is easy to

The associate editor coordinating the review of this manuscript and approving it for publication was Prakasam Periasamy.

access and inexpensive. However, the diagnosis is subjective and has both intra- and inter-observer variations [7], [8]. OCT is a structural investigation. It provides quantitative measurement to overcome the limitations of optic disc examination. The retinal nerve fiber thickness around the optic nerve head in OCT is the most commonly used parameter and provides good diagnostic accuracy for glaucoma detection. However, OCT retinal nerve fiber layer thickness has the limitation in the diagnosis of advanced glaucoma [9]. The retinal nerve fiber layer thickness can also be out of normal range in patients with other retinal pathologies and eye morphology, such as myopia [10], [11], [12]. Visual field is another instrument to measure and monitor visual function, including the depth and extension of visual field defect. However, this is another subjective tool and requires patient's performance and attention. Therefore, it has a lot of unreliable results due to fixation loss, false positive, false negative and other confounding errors.

Recently, OCT angiography (OCTA) has been developed as a non-invasive method to evaluate microvasculopathy and widely used to diagnose and monitor retinal disorders. The principle is to compare the variation between moving objects in blood vessels and surrounding static tissue. In OCTA imaging, the enface image of the region of interest (ROI) is generated [13], [14], [15], [16]. Then a retinal and a choroidal layers are automatically segmented into multiple slabs. At present, there is no consensus on which ROI gives the best indication of glaucoma. So the ROI and the layer of interest are selected by physicians/researchers. Various quantitative parameters have been extracted from the OCTA image for glaucoma diagnosis. Following are the parameters that are found to be comparable with neural component in OCT.

- Blood vessel density is the most explored parameter. Reduction of blood vessels density in optic disc and macular area was correlated with glaucoma severity [17], [18], [19], [20] and retinal nerve fiber layer thinning derived from OCT [21]. It was found that in advanced glaucoma cases, the blood vessels density is a better indicator than the retinal nerve fiber layer thickness [21].
- Foveal avascular zone is an area around the macula that is absent of blood vessel. Previous study found an increase in the area of the foveal avascular zone in glaucoma patients [22]. This finding was correlated with visual field abnormalities. In addition, the foveal avascular zone became less circular in acute angle closure glaucoma [23] and glaucoma with central visual field defect [24].
- Microvascular dropout, found in glaucomatous eyes, is an area that is absent of choroidal blood vessels in β-zone peripapillary area. It was correlated with the reduction of blood vessel density [25], rate of retinal nerve fiber layer thinning [26] and visual field defect [25].

Besides the above parameters, there are other vascular parameters related to glaucoma [27]. For examples, disc flow index, blood vessels tortuosity, vessel perimeter index, vessel complexity, branchpoint analysis, and flow analysis. The relation of these parameters to the glaucoma comes from clinical observation, thus, some image information can be overlooked. Furthermore, the features that were described in previous literature are individually extracted/segmented by tailor-made image processing techniques which is time consuming and may gave an incorrect value in noisy image [28].

Convolutional neural network (CNN) is an effective image classifier. It is trained to automatically capture the image features important for its problem. CNN can be the more effective glaucoma detector, since it can be trained to use the non-clinical features that are correlated with vascular mechanism in the pathogenesis of glaucoma. CNN uses a patch convolved over the entire image. It extracts dominant features in the hidden layers while preserves the correlation between neighboring pixels [29]. After that, the output signal is transformed into a vector and classified. CNN has been applied to many ophthalmologic image modalities. Several studies evaluated the performance of glaucoma detection in the fundus photograph using transfer learning [30], [31], [32], [33] on various conventional deep learning models such as VGG16, VGG19, Inception-v3, ResNet50, and GoogLeNet. The area under receiver operating characteristic curves (AUC) were around 0.90 or more [32], [33], [34]. The results showed the accuracy equal to or more than ophthalmology trainees [34], [35]. Some investigators evaluated the performance of deep learning in OCT retinal nerve fiber layer thickness and found the AUC of more than 0.90 [36], [37], [38]. In addition, a combination of OCT quantitative value to the fundus photograph was another approach to improve the accuracy of glaucoma diagnosis [39].

A number of deep learning methods have been applied to an OCTA image for diagnosing retinal diseases [40], [41], [42]. Nagasato *et al*. [40] applied VGG16 and supported vector machine to detect non-perfusion area in retinal vein occlusion. 322 OCTA images of normal and retinal vein occlusion were augmented and used. The AUC of VGG16 was 0.98 which was better than supported vector machine and ophthalmologists. Le *et al*. [41] also used VGG16 to detect diabetic retinopathy. The VGG16 was trained with a very small dataset (32 controls and 99 diabetic eyes). The best accuracy (AUC of 0.97–0.98) was achieved when the final 9 layers were retrained. Another study on diabetic retinopathy was done by Heisler, *et al*. [42]. They use ensemble method on multiple layers of foveal avascular zone area in 380 eyes and found that VGG19 provided the best performance with an AUC of 0.90–0.92.

The application of deep learning for glaucoma detection in an OCTA image is still limited. Recently, Bowd, *et al*. [43] compared the performance of VGG16 and gradient boosting classifier model in 4.5×4.5 mm^2 of radial peripapillary capillary vessel density layer of optic nerve head image. The weight in the first 4 convolution blocks were frozen

TABLE 1. Demographic data of study sample is 939 eyes from 546 patients to take the OCTA images by the three glaucoma specialists.

Demographic data	Train		Test	
	GL (n = 258)	NG (n = 439)	GL (n = 27)	NG (n = 48)
Age (y); mean (SD)	67.7 (11.0)	62.8 (13.7)	68.5 (5.9)	62.9 (13.3)
Gender; male (%)	47.3	36.0	48.1	35.9
RNFLT (μm); mean (SD)	68.9 (10.4)	88.2 (10.0)	67.4 (9.7)	88.2 (9.9)
VF MD (dB); mean (SD)	-7.5 (7.8)	-2.5 (4.1)	-7.5 (7.3)	-2.4 (4.1)
VF PSD (dB); mean (SD)	6.0 (4.1)	2.8 (2.0)	6.1 (4.4)	2.8 (2.0)

GL; glaucoma group, NG; non-glaucoma group, RNFLT; retinal nerve fiber layer thickness, VF; visual field, MD; mean deviation, PSD; pattern standard deviation, dB; decibel

and the weights in the remaining blocks were retrained. The performance of VGG16 was better than gradient boosting classifier model that derived from the OCTA machine. They also implemented other deep learning models and found to be better than gradient boosting classifier.

In this paper, we applies CNN to diagnose glaucoma from OCTA images. We hypothesized that the prominent of retinal vessels in OCTA image enhances the visibility of the neural network for glaucoma classification. In addition, the role of vascular mechanism in glaucoma pathogenesis may be important. Instead of focusing only at the optic disc, we expand our ROI to the surrounding retina and macular regions. The OCTA imaging is among the recent imaging modalities. We found only one public OCTA database [44]. However, optic nerve head images are not routinely included. In this paper, we proposes GlauNet to capture the glaucoma features from limited data. The architecture of GlauNet was based on our previous researches [45], [46] which shows that the shallow convolutional networks is efficient in the analysis of medical imaging. In the experiment on glaucoma detection, the proposed GlauNet is compared with the classic VGG16 and ResNet50 and recently proposed, EfficientNetV2 to classify glaucoma from OCTA images.

II. METHODOLOGY

A. STUDY SETTING AND POPULATION

The retrospective study was conducted at the Department of Ophthalmology, Faculty of Medicine, Chulalongkorn University and King Chulalongkorn Memorial Hospital, Bangkok, Thailand. The Institutional Review Board of the Faculty of Medicine, Chulalongkorn University according to the declaration of Helsinki approved the protocol. The inclusion criteria was patients presenting to the eye clinic who were over 18 years old and underwent OCTA, optic disc photograph and/or OCT and visual field test results within 6 months from each other during January 2018 to October 2021. The demographic of our data is shown in Table 1. The exclusion criterion was poor quality OCTA images, including eye movement, defocus, shadow, banding, segmentation error, blink, or Z offset in at least 10% of the image area [47], [48], [49]. However, we did not exclude an eye with decentration if the image still contained optic nerve head and macula. The poor quality images were later used to evaluate the proposed GlauNet regarding the robustness against artifacts.

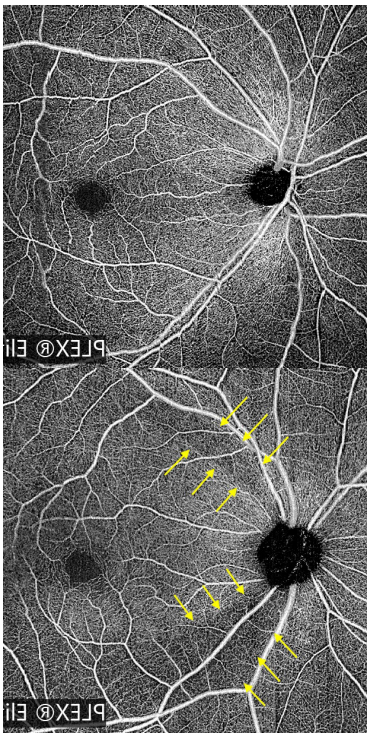

FIGURE 1. An example of optical coherence tomography angiography (OCTA) images consists of (top) a normal or non-glaucoma eye image and (bottom) a glaucomatous eye image which were flipped to the right eye format. (Yellow arrows: area of retinal vessel density reduction in glaucomatous eye).

B. GROUND TRUTH

To set the ground truth, three glaucoma specialists (SC, KR, NU) independently graded optic disc photographs in conjunction with OCT and/or visual field results and made a diagnosis to be normal, glaucoma suspect or glaucoma. The criteria for glaucoma (GL) diagnosis were adapted from Li, *et al*. [32]. Normal visual field was determined by glaucoma hemifield test within normal limits and and pattern standard deviation more than 5%. The final diagnosis depended upon majority vote. If the majority vote is not reached, a senior expert (AM) independently reviewed the investigation results and made a diagnosis. The normal and suspected eyes were grouped into non-glaucoma (NG) group. The data were divided into training and test datasets. The demographics of the training and test datasets are shown in Table 1.

C. DATA ACQUISITION AND IMAGE PRE-PROCESSING

This research collected OCTA images of the whole retinal layers with a size of 15×9 mm^2 that was equivalent to 1024×614 pixels in RGB format from Zeiss PLEX® Elite 9000 (Software version 2.1.0.55513; Carl Zeiss Meditec, Dublin, CA, USA). To reduce the computational time and get rid of

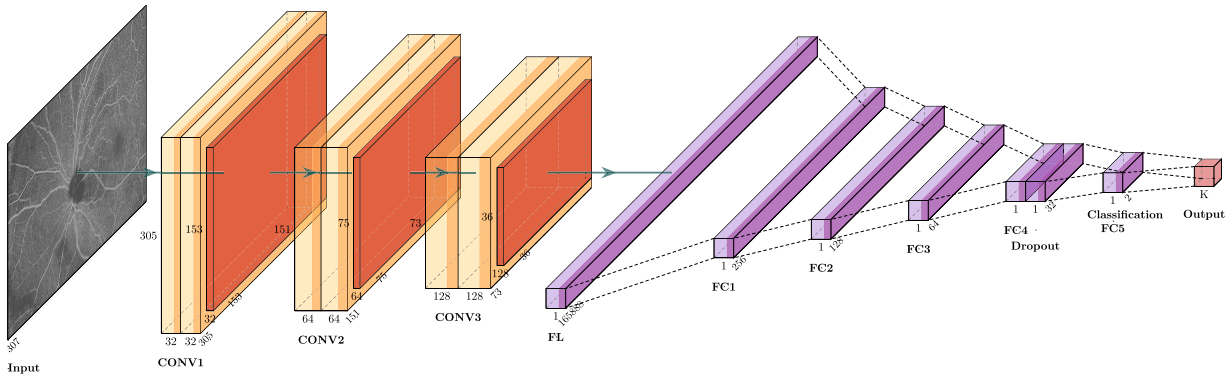

FIGURE 2. The overall proposed architecture of a new convolution neural network for intelligent glaucoma diagnosis on OCTA images (GlauNet) consists of two sections: feature-extraction section consisting of three convolutional layers(*CONV*) where each layer is followed by the rectified linear unit (*ReLU*) and the maximum pooling filtering (*MP*) and classification section consisting of five fully connected (*FC*) layers.

artifacts that usually appear on both sides of an OCTA image, all images were cropped to 614 × 614 pixels such that they still contained optic disc and macula. All left-eye images were horizontal flipped to the right-eye format, as shown in Fig. 1. We used stratified random sampling to separate the dataset at the participants level into 90% for training and 10% for testing. All images were normalized from a range of 0–255 to 0–1. The input OCTA image was then resized to 307 × 307 × 3 pixels. The training dataset was augmented by applying horizontal flip, rotation (0–7 degree), width and height shifts (0%–5%) and brightness adjustment (80%–100%). In the training dataset, 5-fold cross validation was used to find the best architecture as well as the hyperparameters. Therefore, the ratio between training and validation data was set to 80:20.

D. GlauNet

In this paper, the new CNN architecture for glaucoma diagnosis from an OCTA image, namely GlauNet, is proposed. The overall architecture of GlauNet is shown in Fig. 2. It has two sections: feature-extraction section and classification section. Its input image, I_{input}, is an 307 × 307 × 3 OCTA images as shown in Fig. 3(a).

The feature-extraction section consists of three convolutional layers and one flatten layer. In the convolutional layer (*CONV*), the outputs of the previous layer are filtered according to the following equation.

$$z^t = h^{t-1} * W^l \tag{1}$$

where z^t is the pre-activation output of layer t; h^t is the output of layer t; $*$ is the discrete convolution operator; W^t is the learnable $n \times n$ parameters of layer t and can be considered as the adaptive kernel function. The convolution layer is followed by rectified linear unit (*ReLU*), which provides the output (Z_i) according to the following equation.

$$ReLU(Z_i) = max(0, z_i). \tag{2}$$

The maximum pooling layers (*MP*) seeks the strongest response inside the $s \times s$ windows and can be formulated as follows.

$$h^t_{xy} = max_{i=0,\ldots,s,j=0,\ldots,s} Z^{t-1}_{(x+1)(y+1)}, \tag{3}$$

where h^t_{xy} is the output of layer t at (x, y) and $Z^{t-1}_{(x+i)(y+j)}$ is the output of *ReLU* unit in the previous layer.

All *MP* layers have the size of 2 × 2 with the stride of 2. The first convolutional layer (*CONV1*) contains a stack of 32 convolution filters with the 3 × 3 kernel size. It was followed by *ReLU1* and *MP1*. The output of *MP1* was 32 153 × 153 images. Fig. 3(b) shows the sample outputs of this layer for a glaucomatous and a non-glaucomatous eyes. The second convolutional layer (*CONV2*) contains a stack of 64 3 × 3 convolution filters. The output of the second layer after *MP2* is 64 75 × 75 images. Fig. 3(c) shows the sample outputs of the glaucomatous and non-glaucomatous images. The last convolutional layer (*CONV3*) contains a stack of 128 3 × 3 convolution filters. The output after *MP3* is 128 36 × 36 images. The sample outputs are shown in Fig. 3(d), respectively.

128 output images are grouped and vectorized into a 1 × 165, 888 vector. The vectorization is represented as a flatten layer (*FL*) in Fig. 2. The architecture of the feature-extraction section can be written in the formulated form of the neural network model as follows:

$$\begin{aligned} GlauNet^{F.E.} &= I_{input}(N, N, 3) \\ &\rightarrow CONV1(3, 3, 32) \rightarrow ReLU1 \rightarrow MP1(2, 2) \\ &\rightarrow CONV2(3, 3, 64) \rightarrow ReLU2 \rightarrow MP2(2, 2) \\ &\rightarrow CONV3(3, 3, 128) \rightarrow ReLU3 \rightarrow MP3(2, 2) \\ &\rightarrow FL. \end{aligned} \tag{4}$$

The classification section consists of five fully connected layers (*FC*). All outputs in the previous layer are linearly convoluted as follows.

$$z^l = W^l h^{l-1}. \tag{5}$$

The sizes of the five layers are 256 (*FC1*), 128 (*FC2*), 64 (*FC3*), 32 (*FC4*) and 2 (*FC5*) nodes. To avoid overfitting, the *FC4* layer has the dropout rate of 0.5. There are

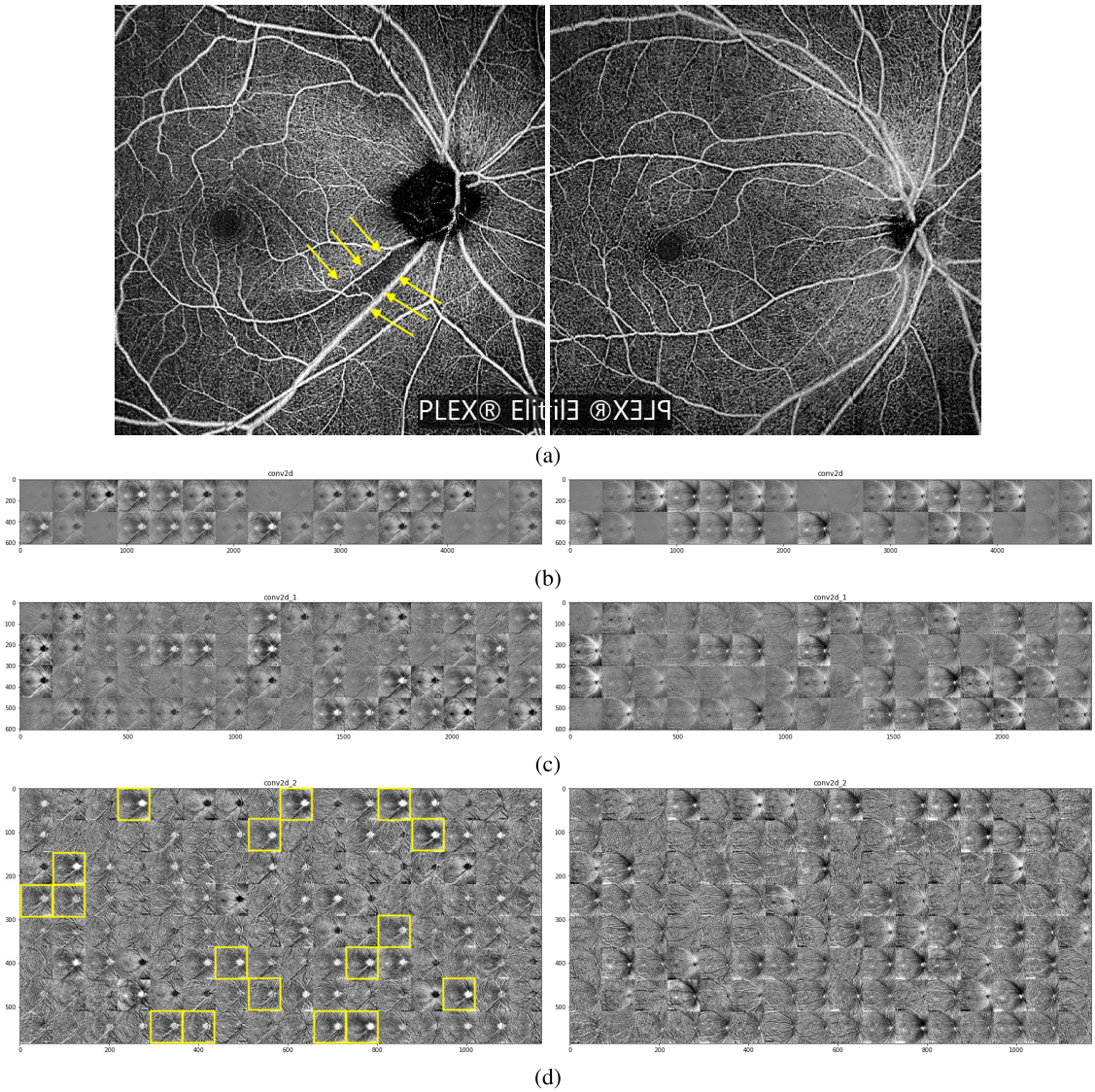

FIGURE 3. Visualization of feature map in GlauNet model of each convolutional layer in (a:left) glaucomatous and (a:right) non-glaucomatous eyes with (b), (c), and (d) represent the example results of *CONV1*, *CONV2*, and *CONV3* from glaucomatous and non-glaucomatous images, respectively.

42,467,584 connected parameters from flatten data. The *FC5* layer has 2 nodes: one for glaucomatous and the other for non-glaucomatous eyes. The activation function of *FC* is a sigmoid function. The proposed GlauNet can be represented by the following formulated form:

$$\begin{aligned} GlauNet &= GlauNet^{F.E.} \\ &\rightarrow FC1(256) \rightarrow FC2(128) \\ &\rightarrow FC3(64) \rightarrow FC4(32) \\ &\rightarrow FC5(2). \end{aligned} \tag{6}$$

An OCTA image was classified as low-quality image if it contains one of the following artifacts in at least 10% of the image.

- Eye movement
- Defocus
- Shadow
- Banding
- Segmentation error
- Blink
- Z offset

Low-quality images were excluded from the training of GlauNet as well as for the evaluation of the best architecture and hyperparameters. However, a subset of low-quality images that contained optic nerve head and macula was used to test for the robustness against artifacts.

E. STATISTICAL ANALYSIS

The evaluation of GlauNet was based on 8 diagnostic test parameters: sensitivity, specificity, positive and negative predictive values (PPV and NPV), likelihood ratio of positive (LR+) and negative tests (LR−), accuracy and area under receiver operator characteristic curve (AUC). The expert opinion is considered as a ground truth. All statistical analysis was performed using STATA software version 15.1 (StataCorp LLC). Definitions of all parameters are shown below.

Sensitivity is a true positive in the patient (positive) group.

$$Sensitivity = \frac{TP}{TP + FN} \tag{7}$$

Specificity is a true negative in the control (negative) group.

$$Specificity = \frac{TN}{TN + FP} \tag{8}$$

Positive predictive value (PPV) is the collection of patients who have test positive.

$$PPV = \frac{TP}{TP + FP} \tag{9}$$

Negative predictive value (NPV) is the collection of controls who have test negative.

$$NPV = \frac{TN}{TN + FN} \tag{10}$$

Likelihood ratio of positive test (LR+) indicated the degree that the test is more likely to be positive in disease than controls. A higher value determines ability of the test to rule in a disease. LR+ is defined as follows.

$$LR+ = \frac{TP/(TP + FN)}{FP/(TN + FP)} \tag{11}$$

In the contrary, likelihood ratio of negative test (LR –) indicates the degree that the test is less likely to be negative in disease than controls. A lower value determines ability of the test to rule out a disease.

$$LR- = \frac{FN/(TP + FN)}{TN/(TN + FP)} \tag{12}$$

Accuracy means the ratio of correct classification to the number of included cases.

$$Accuracy = \frac{TP + TN}{TP + FP + FN + TN} \tag{13}$$

III. EXPERIMENTAL RESULTS

939 OCTA images were taken from 546 patients. One hundred and sixty-seven images (17.8%) were excluded from the training process due to poor image quality. Therefore, the dataset in the experiment composed of 285 GL and 487 NG eyes. Demographic of the samples is shown in Table 1. There were 258 GL and 439 NG eyes in the training set and 27 GL and 48 NG eyes in the test set. GlauNet was compared with VGG16, ResNet50, and EfficientNetV2.

A. GlauNet PARAMETERS SETTING

We divided the study group at the participant level into 2 groups: 90% for training and 10% for testing. In the training group, the ratio of the training and the validation images was set to 4:1. Five-fold cross validation was applied to the training group to find the best architecture and hyperparameters. Adams optimizer was used. The accuracy was evaluated from the validation images. The batch size was varied from 16 to 300. The training rate was varied from 0.01 to 0.00001 for finding the best setting. It was found that the architecture in Fig. 2. provided the highest accuracy. The best hyperparameter of GlauNet was set as followed: batch size 200, learning rate 0.0001, and trained for 100 epochs.

B. DIAGNOSTIC PERFORMANCE

The accuracy of the GlauNet with 5-fold cross validation for the training set varied between 85.30% and 90.11%. For the test set, the accuracy ranged from 79.86% to 87.05%. One example of the accuracy and loss graph was shown in Fig. 4. In our experiment, only GlauNet was capable of differentiating glaucomatous and normal eyes. VGG16, ResNet50 and EfficientNetV2 failed to learn and classified images either as all normal or all glaucomatous eyes.

The visualization of the feature extraction in GlauNet was shown in Fig. 3. The most highlighted area was the optic disc and superotemporal and inferotemporal area. Yellow arrow in Fig. 3(a:left) show the area with a decrease in vessel density. The macula was highlighted only in the first convolutional layer and became less prominent afterwards. In glaucomatous eye, the loss of retinal vessel density was highlighted in the last convolution layer, as shown inside the yellow rectangle in Fig. 3(d:left). This finding was correlated with clinical observation that found reduction of retinal vessel density in the affected area (between arrows in Fig. 3(a:left)). This finding was not presented in nonglaucomatous eye with the same filter, as shown in Fig. 3(d:right).

C. MODEL EVALUATION

The test set was augmented in the same manner as the training set in order to evaluate the robustness against the change in camera setting. The performance of GlauNet for the test set and the augmented test set was shown in Table 2. There was only a slight difference between the performance in these two test sets, so it can be concluded that GlauNet was robust against the change in camera setting. In the test set, the classification by other three CNNs were poor. All eyes were classified as glaucoma.

The predictive values in Table 2 can be used to explain the probability of getting the correct diagnosis. GlauNet had 93.5% negative predictive value. This meant that if an image was classified as non-glaucomatous, the probability of the image being non-glaucomatous would be more than 90%. The likelihood ratio of positive test (LR+) of 8.06 implied that the probability of the image being glaucomatous was moderately increased when the input was classified as glaucoma. Furthermore, the likelihood ratio of negative test (LR –) of 0.12 meant that the probability of the image being non-glaucomatous was moderately decreased when the input was classified as glaucoma.

There were 8 (10.1%) and 45 (10.0%) misclassified images in the test and the augmented test set, respectively. The numbers of false negatives were 3 and 30. The numbers of false positives were 5 and 15.

GlauNet was also tested for the robustness against OCTA artifacts. Poor-quality images that still contained optic nerve head and macula were used as the testing images. Out of

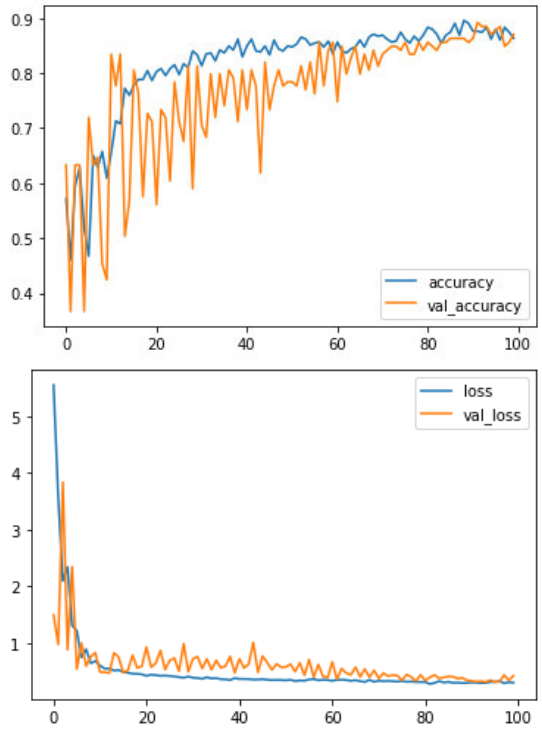

FIGURE 4. Training and validate results of GlauNet model represent the accuracy and loss values from the training and validate dataset.

TABLE 2. Performance of GlauNet for glaucoma diagnosis from an OCTA image.

Model	Test set	Augmented test set	Poor quality images
Sensitivity (%)	88.9	90.1	82.4
Specificity (%)	89.6	86.5	80.3
PPV (%)	82.8	78.9	50.0
NPV (%)	93.5	94.0	95.0
LR+	8.06	8.75	4.55
LR-	0.12	0.15	0.24
Accuracy (%)	89.3	87.8	80.7
AUC (95%CI)	0.89 (0.82 - 0.97)	0.88 (0.85 - 0.91)	0.81 (0.71 - 0.92)

PPV; Positive predictive value, NPV; Negative predictive value, LR+; Likelihood ratio for positive test, LR-; Likelihood ratio for negative test, AUC; Area under receiver operating characteristic curve

167 poor quality images, 88 images met our criterion. There were 17 GL and 71 NG eyes. The result was shown in Table 2. Though there was some drop in performance, but the sensitivity, specificity and accuracy were still more than 80%. Example of poor quality images and their classifications are shown in Fig. 5. The robustness against artifacts were not investigated for VGG16, ResNet50 and EfficientNetV2, because these three CNNs failed even in images without artifacts.

IV. DISCUSSION

In this study, we evaluated the performance of CNN to detect glaucoma from OCTA images. OCTA is a new tool for glaucoma diagnosis, therefore, a large image database has not been available yet. We developed a customized CNN model, namely GlauNet. GlauNet contained 3 convolutional layers and was applied to the dataset with 697 eyes in the training

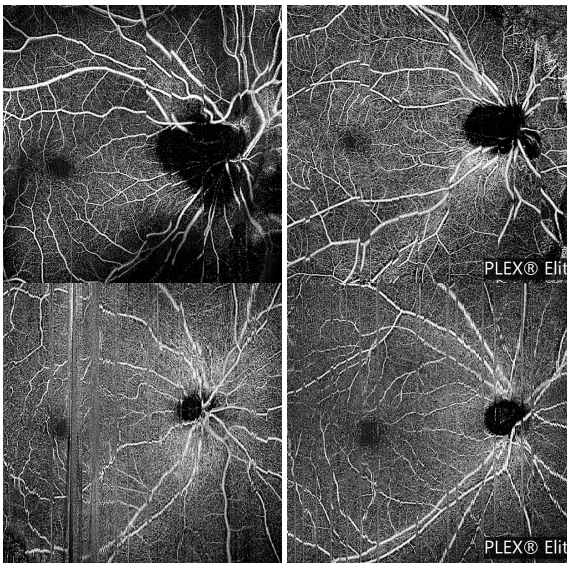

FIGURE 5. Example of poor quality images that were predicted by GlauNet. Top left; true positive in glaucomatous eye, Top right; false negative in glaucomatous eye, bottom left; true negative in non-glaucomatous eye, bottom right; false positive in non-glaucomatous eyes.

set and 75 eyes in the test set. Only our proposed GlauNet was capable of differentiating between glaucomatous and non-glaucomatous eyes. The moderate high likelihood ratio value of GlauNet indicated that it was applicable to large dataset (general population).

VGG16 and ResNet50 with transfer learning have been applied to OCTA images to detect retinal vein occlusion [40], diabetic retinopathy [41], [42] and glaucoma [43]. They provided excellent results. However, pre-trained networks did not work well with our data. The primary reason would be a limited dataset. To deal with this issue, previous reports modified the training steps to fit their data [40], [41], [42], [43]. Another possible explanation was the distinct difference between normal eyes and eyes with diabetic retinopathy or retinal vein occlusion. The first character was the broadening of white area with distinct border, such as retinal vessel thickening and microaneurysm in diabetic retinopathy. The second character was the black area inside the white retina area. The black area was the result of the capillary loss in diabetic retinopathy and non-perfusion area in retinal vein occlusion [40], [42]. Both characters are prominent and easy to identify, whereas the change of retinal vessels in a glaucoma eye is gradual and sometimes has ill-defined border.

Recently, Bowd, *et, al.* [43] applied modified VGG16 to the peripapillary OCTA images and found the areas under precision-recall curves of 0.97. In this study, we used wider field of OCTA image that included retinal and capillary vessels outside the peripapillary area because the correlation between foveal avascular zone and glaucoma was reported in [22], [23], [24]. In addition, because the prevalence of poor image quality was high [47], [48], [49], wider field of view that includes more clinical important area may provide more data for CNN to learn and predict in less severe case of poor quality image. We evaluated the generalization of

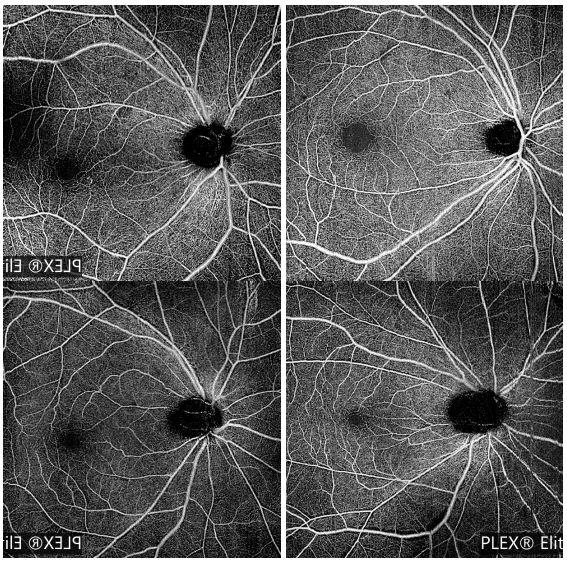

FIGURE 6. Example of misclassified OCTA images. Top; false negative in glaucomatous eyes, bottom; false positive in non-glaucomatous eyes.

the GlauNet model by comparing the performance in test and augmented test sets which showed similar results. Also, we found good performance of GlauNet in poor quality images that usually excluded in previous studies, as represented in Table 2.

Our model found misclassification in about 10% of both test and augmented-test images. The examples are shown in Fig. 6. False negative results were found in images with less or absence of retinal vessel density reduction area. The false positive images were presented in images that contained shadow and/or the mimic of retinal vessel reduction due to the brightness reduction. This finding was not similar to the training in optic disc photograph that found false positive results in eyes with other retinal conditions [32]. In this study, we did not exclude other eye diseases or patients who underwent intraocular surgery to make the model more generalized. However, to be included in the study, the patients need to have OCTA, and optic disc photograph within 6 months. Therefore, there were only 72 (9.3%) eyes with other ocular disorders. However, our proposed GlauNet correctly classified these 72 images.

There are some limitations in our study. OCTA is a new tool compared to optic disc photograph or OCT, therefore, we still lack a large dataset. The only OCTA public dataset focuses on the macula area that does not match our purpose. Glaucoma mostly affect retina area in macular and optic disc. Even with small dataset with image augmentation, the proposed GlauNet still provided a very good accuracy in the test set. Furthermore, we developed this CNN architecture based on the image from only one OCTA instrument. The performance in other machines needed to be explored. In addition, OCTA vascular structure for glaucoma diagnosis is an on-going research and it is not generally available in most ophthalmology clinics. However, if the vascular cause has a significant role, we may need to combine this finding with the current examination of neural structure.

V. CONCLUSION

GlauNet was proposed for glaucoma diagnosis based on an OCTA image. It was trainable with small dataset and robust against different camera projection setting as well as image artifacts. The robustness can be further improved if actual data with more variation are used for training. Variation comes from both patients (ethnicities, severity, etc.) and OCTA instruments (manufacturer, setting, etc.). Currently, the input of GlauNet is retinal vessels in all layers of the OCTA image. However, some layers may be more correlated to glaucoma than the others. The correlation between the specific layer and glaucoma should be further investigated for both the understanding of the disease and better classification.

REFERENCES

[1] Y. C. Tham, X. Li, T. Y. Wong, H. A. Quigley, T. Aung, and C. Y. Cheng, "Global prevalence of glaucoma and projections of glaucoma burden through 2040. A systematic review and meta-analysis," *Ophthalmology*, vol. 121, no. 11, pp. 2081–2090, Nov. 2014.

[2] A. J. W. King, A. Reddy, J. R. Thompson, and A. R. Rosenthal, "The rates of blindness and of partial sight registration in glaucoma patients," *Eye*, vol. 14, no. 4, pp. 613–619, Jul. 2000.

[3] H. A. Quigley, S. K. West, J. Rodriguez, B. Munoz, R. Klein, and R. Snyder, "The prevalence of glaucoma in a population-based study of Hispanic subjects: Proyecto VER," *Arch. Ophthalmol.*, vol. 119, no. 12, pp. 1819–1826, Dec. 2001.

[4] A. P. Rotchford, J. F. Kirwan, M. A. Müller, G. J. Johnson, and P. Roux, "Temba glaucoma study: A population-based cross-sectional survey in urban south Africa," *Ophthalmology*, vol. 110, no. 2, pp. 376–382, Feb. 2003.

[5] A. Hennis, S. Y. Wu, B. Nemesure, R. Honkanen, and M. C. Leske, "Awareness of incident open-angle glaucoma in a population study: The Barbados Eye Studies," *Ophthalmology*, vol. 114, no. 10, pp. 1816–1821, Oct. 2007.

[6] P. Gupta, D. Zhao, E. Guallar, F. Ko, M. V. Boland, and D. S. Friedman, "Prevalence of glaucoma in the United States: The 2005–2008 national health and nutrition examination survey," *Invest. Ophthalmol. Vis. Sci.*, vol. 57, no. 6, pp. 2905–2913, May 2016.

[7] H. D. Jampel, D. Friedman, H. Quigley, S. Vitale, R. Miller, F. Knezevich, and Y. Ding, "Agreement among glaucoma specialists in assessing progressive disc changes from photographs in open-angle glaucoma patients," *Amer. J. Ophthalmol.*, vol. 147, no. 1, pp. 39–44, Jan. 2009.

[8] C. Breusegem, S. Fieuws, I. Stalmans, and T. Zeyen, "Agreement and accuracy of non-expert ophthalmologists in assessing glaucomatous changes in serial stereo optic disc photographs," *Ophthalmology*, vol. 118, no. 4, pp. 742–746, Apr. 2011.

[9] C. Bowd, L. M. Zangwill, R. N. Weinreb, F. A. Medeiros, and A. Belghith, "Estimating optical coherence tomography structural measurement floors to improve detection of progression in advanced glaucoma," *Amer. J. Ophthalmol.*, vol. 175, pp. 37–44, Mar. 2017.

[10] K. E. Kim, J. W. Jeoung, K. H. Park, D. M. Kim, and S. H. Kim, "Diagnostic classification of macular ganglion cell and retinal nerve fiber layer analysis: Differentiation of false-positives from glaucoma," *Ophthalmology*, vol. 122, no. 3, pp. 502–510, Mar. 2015.

[11] S. Biswas, C. Lin, and C. K. S. Leung, "Evaluation of a myopic normative database for analysis of retinal nerve fiber layer thickness," *JAMA Ophthalmol.*, vol. 134, no. 9, pp. 1032–1039, Sep. 2016.

[12] A. Manassakorn, K. Khamwan, D. Owasirikul, R. Itthipanichpong, V. Sa-Ing, and S. Auethavekiat, "Retinal nerve fiber layer defect detection using machine learning on optic disc photograph," in *Proc. IEEE EMBS Int. Conf. Biomed. Health Informat. (BHI)*, Jul. 2021, pp. 1–4.

[13] S. S. Gao, Y. Jia, M. Zhang, J. P. Su, G. Liu, T. S. Hwang, S. T. Bailey, and D. Huang, "Optical coherence tomography angiography," *Invest. Ophthalmol. Vis. Sci.*, vol. 57, no. 9, pp. 27–36, Jul. 2016.

[14] C.-L. Chen and R. K. Wang, "Optical coherence tomography based angiography [invited]," *Biomed. Opt. Exp.*, vol. 8, no. 2, pp. 1056–1082, 2017.

[15] S. Chansangpetch and S. C. Lin, "Optical coherence tomography angiography in glaucoma care," *Current Eye Res.*, vol. 43, no. 9, pp. 1067–1082, Sep. 2018.
[16] A. Harris, G. Guidoboni, B. Siesky, S. Mathew, A. C. Verticchio Vercellin, L. Rowe, and J. Arciero, "Ocular blood flow as a clinical observation: Value, limitations and data analysis," *Prog. Retinal Eye Res.*, vol. 78, Sep. 2020, Art. no. 100841.
[17] A. Yarmohammadi, L. M. Zangwill, A. Diniz-Filho, M. H. Suh, P. I. Manalastas, N. Fatehee, S. Yousefi, A. Belghith, L. J. Saunders, F. A. Medeiros, D. Huang, and R. N. Weinreb, "Optical coherence tomography angiography vessel density in healthy, glaucoma suspect, and glaucoma eyes," *Investigative Opthalmol. Vis. Sci.*, vol. 57, no. 9, Jul. 2016, Art. no. OCT451.
[18] L. S. Geyman, R. A. Garg, Y. Suwan, V. Trivedi, B. D. Krawitz, S. Mo, A. Pinhas, A. Tantraworasin, T. Y. P. Chui, R. Ritch, and R. B. Rosen, "Peripapillary perfused capillary density in primary open-angle glaucoma across disease stage: An optical coherence tomography angiography study," *Brit. J. Ophthalmol.*, vol. 101, no. 9, pp. 1261–1268, Sep. 2017.
[19] H. L. Rao, Z. S. Pradhan, R. N. Weinreb, M. Riyazuddin, S. Dasari, J. P. Venugopal, N. K. Puttaiah, D. A. S. Rao, S. Devi, K. Mansouri, and C. A. B. Webers, "A comparison of the diagnostic ability of vessel density and structural measurements of optical coherence tomography in primary open angle glaucoma," *PLoS ONE*, vol. 12, no. 3, Mar. 2017, Art. no. e0173930.
[20] S. Moghimi, L. M. Zangwill, R. C. Penteado, K. Hasenstab, E. Ghahari, H. Hou, M. Christopher, A. Yarmohammadi, P. I. C. Manalastas, T. Shoji, C. Bowd, and R. N. Weinreb, "Macular and optic nerve head vessel density and progressive retinal nerve fiber layer loss in glaucoma," *Ophthalmology*, vol. 125, no. 11, pp. 1720–1728, Nov. 2018.
[21] H. L. Rao, Z. S. Pradhan, R. N. Weinreb, M. Riyazuddin, S. Dasari, J. P. Venugopal, N. K. Puttaiah, D. A. S. Rao, S. Devi, K. Mansouri, and C. A. B. Webers, "Vessel density and structural measurements of optical coherence tomography in primary angle closure and primary angle closure glaucoma," *Amer. J. Ophthalmol.*, vol. 177, pp. 106–115, May 2017.
[22] R. Igarashi, S. Ochiai, T. Togano, Y. Sakaue, A. Suetake, R. Iikawa, Y. Honma, D. Miyamoto, and T. Fukuchi, "Foveal avascular zone measurement via optical coherence tomography angiography and its relationship with the visual field in eyes with open-angle glaucoma," *J. Glaucoma*, vol. 29, no. 6, pp. 492–497, Jun. 2020.
[23] K. Liu, H. Xu, H. Jiang, H. Wang, P. Wang, Y. Xu, F. Li, B. Xu, X. Yao, and J. Zou, "Macular vessel density and foveal avascular zone parameters in patients after acute primary angle closure determined by OCT angiography," *Sci. Rep.*, vol. 10, no. 1, p. 18717, Oct. 2020.
[24] J. Kwon, J. Choi, J. W. Shin, J. Lee, and M. S. Kook, "Alterations of the foveal avascular zone measured by optical coherence tomography angiography in glaucoma patients with central visual field defects," *Invest. Ophthalmol. Vis. Sci.*, vol. 58, no. 3, pp. 1637–1645, Mar. 2017.
[25] M. H. Suh, L. M. Zangwill, P. I. C. Manalastas, A. Belghith, A. Yarmohammadi, F. A. Medeiros, A. Diniz-Filho, L. J. Saunders, and R. N. Weinreb, "Deep retinal layer microvasculature dropout detected by the optical coherence tomography angiography in glaucoma," *Ophthalmology*, vol. 123, no. 12, pp. 2509–2518, Dec. 2016.
[26] J. A. Kim, E. J. Lee, and T. W. Kim, "Evaluation of parapapillary choroidal microvasculature dropout and progressive retinal nerve fiber layer thinning in patients with glaucoma," *JAMA Ophthalmol.*, vol. 137, no. 7, pp. 810–816, Jul. 2019.
[27] X. Yao, M. N. Alam, D. Le, and D. Toslak, "Quantitative optical coherence tomography angiography: A review," *Exp. Biol. Med. (Maywood)*, vol. 245, no. 4, pp. 301–312, Feb. 2020.
[28] N. M. Zaitouna and M. J. Aqelb, "Survey on image segmentation techniques," *Proc. Comput. Sci.*, vol. 65, pp. 797–806, Jan. 2015.
[29] Y. LeCun, Y. Bengio, and G. Hinton, "Deep learning," *Nature*, vol. 521, no. 7553, pp. 436–444, Sep. 2015.
[30] A. Li, J. Cheng, D. W. K. Wong, and J. Liu, "Integrating holistic and local deep features for glaucoma classification," in *Proc. 38th Annu. Int. Conf. IEEE Eng. Med. Biol. Soc. (EMBC)*, Aug. 2016, pp. 1328–1331.
[31] A. Cerentini, D. Welfer, M. C. d'Ornellas, C. J. Pereira Haygert, and G. N. Dotto, "Automatic identification of glaucoma using deep learning methods," *Stud. Health Technol. Inform.*, vol. 245, pp. 318–321, 2017.
[32] Z. Li, Y. He, S. Keel, W. Meng, R. Chang, and M. He, "Efficacy of a deep learning system for detecting glaucomatous optic neuropathy based on color fundus photographs," *Ophthalmology*, vol. 125, no. 8, pp. 1199–1206, 2018.
[33] M. Christopher, A. Belghith, C. Bowd, J. A. Proudfoot, M. H. Goldbaum, R. N. Weinreb, C. A. Girkin, J. M. Liebmann, and L. M. Zangwill, "Performance of deep learning architectures and transfer learning for detecting glaucomatous optic neuropathy in fundus photographs," *Sci. Rep.*, vol. 8, no. 1, Nov. 2018, Art. no. 16685.
[34] N. Shibata, M. Tanito, K. Mitsuhashi, Y. Fujino, M. Matsuura, H. Murata, and R. Asaoka, "Development of a deep residual learning algorithm to screen for glaucoma from fundus photography," *Sci. Rep.*, vol. 8, no. 1, p. 14665, Oct. 2018.
[35] S. Phene, R. C. Dunn, N. Hammel, Y. Liu, J. Krause, N. Kitade, M. Schaekermann, R. Sayres, D. J. Wu, A. Bora, C. Semturs, A. Misra, A. E. Huang, A. Spitze, F. A. Medeiros, A. Y. Maa, M. Gandhi, G. S. Corrado, L. Peng, and D. R. Webster, "Deep learning and glaucoma specialists: The relative importance of optic disc features to predict glaucoma referral in fundus photographs," *Ophthalmology*, vol. 126, no. 12, pp. 1627–1639, 2019.
[36] A. R. Ran, C. Y. Cheung, X. Wang, H. Chen, L.-Y. Luo, P. P. Chan, M. O. M. Wong, R. T. Chang, S. S. Mannil, A. L. Young, H.-W. Yung, C. P. Pang, P.-A. Heng, and C. C. Tham, "Detection of glaucomatous optic neuropathy with spectral-domain optical coherence tomography: A retrospective training and validation deep-learning analysis," *Lancet Digit. Health*, vol. 1, no. 4, pp. e172–e182, Aug. 2019.
[37] S. Maetschke, B. Antony, H. Ishikawa, G. Wollstein, J. Schuman, and R. Garnavi, "A feature agnostic approach for glaucoma detection in OCT volumes," *PLoS ONE*, vol. 14, no. 7, Jul. 2019, Art. no. e0219126.
[38] A. C. Thompson, A. A. Jammal, S. I. Berchuck, E. B. Mariottoni, and F. A. Medeiros, "Assessment of a segmentation-free deep learning algorithm for diagnosing glaucoma from optical coherence tomography scans," *JAMA Ophthalmol.*, vol. 138, no. 4, pp. 333–339, Apr. 2020.
[39] F. A. Medeiros, A. A. Jammal, and A. C. Thompson, "From machine to machine: An OCT-trained deep learning algorithm for objective quantification of glaucomatous damage in fundus photographs," *Ophthalmology*, vol. 126, no. 4, pp. 513–521, Apr. 2019.
[40] D. Nagasato, H. Tabuchi, H. Masumoto, H. Enno, N. Ishitobi, M. Kameoka, M. Niki, and Y. Mitamura, "Automated detection of a nonperfusion area caused by retinal vein occlusion in optical coherence tomography angiography images using deep learning," *PLoS ONE*, vol. 14, no. 11, Nov. 2019, Art. no. e0223965.
[41] D. Le, M. Alam, C. K. Yao, J. I. Lim, Y.-T. Hsieh, R. V. P. Chan, D. Toslak, and X. Yao, "Transfer learning for automated OCTA detection of diabetic retinopathy," *Transl. Vis. Sci. Technol.*, vol. 9, no. 2, p. 35, Jul. 2020.
[42] M. Heisler, S. Karst, J. Lo, Z. Mammo, T. Yu, S. Warner, D. Maberley, M. F. Beg, E. V. Navajas, and M. V. Sarunic, "Ensemble deep learning for diabetic retinopathy detection using optical coherence tomography angiography," *Transl. Vis. Sci. Technol.*, vol. 9, no. 2, p. 20, Apr. 2020.
[43] C. Bowd, A. Belghith, L. M. Zangwill, M. Christopher, M. H. Goldbaum, R. Fan, J. Rezapour, S. Moghimi, A. Kamalipour, H. Hou, and R. N. Weinreb, "Deep learning image analysis of optical coherence tomography angiography measured vessel density improves classification of healthy and glaucoma eyes," *Amer. J. Ophthalmol.*, vol. 236, pp. 298–308, Apr. 2022.
[44] M. Li, Y. Chen, Z. Ji, K. Xie, S. Yuan, Q. Chen, and S. Li, "Image projection network: 3D to 2D image segmentation in OCTA images," *IEEE Trans. Med. Imag.*, vol. 39, no. 11, pp. 3343–3354, Nov. 2020, doi: 10.1109/TMI.2020.2992244.
[45] V. Sa-Ing, P. Vorasayan, N. C. Suwanwela, S. Auethavekiat, and C. Chinrungrueng, "Real-time 3D ultrasound denoising based on adaptive regularisation Savitzky–Golay filter," *Electron. Lett.*, vol. 53, no. 15, pp. 1029–1031, Jul. 2017.
[46] V. Sa-Ing, P. Vorasayan, N. C. Suwanwela, S. Auethavekiat, and C. Chinrungrueng, "Multiscale adaptive regularisation Savitzky–Golay method for speckle noise reduction in ultrasound images," *IET Image Process.*, vol. 12, no. 1, pp. 105–112, Jan. 2018.
[47] K. Ghasemi Falavarjani, M. Al-Sheikh, H. Akil, and S. R. Sadda, "Image artefacts in swept-source optical coherence tomography angiography," *Brit. J. Ophthalmol.*, vol. 101, no. 5, pp. 564–568, May 2017.
[48] I. C. Holmen, S. M. Konda, J. W. Pak, K. W. McDaniel, B. Blodi, K. E. Stepien, and A. Domalpally, "Prevalence and severity of artifacts in optical coherence tomographic angiograms," *JAMA Ophthalmol.*, vol. 138, no. 2, pp. 119–126, 2020.
[49] A. Kamalipour, S. Moghimi, H. Hou, R. C. Penteado, W. H. Oh, J. A. Proudfoot, N. El-Nimri, E. Ekici, J. Rezapour, L. M. Zangwill, C. Bowd, and R. N. Weinreb, "OCT angiography artifacts in glaucoma," *Ophthalmology*, vol. 128, no. 10, pp. 1426–1437, Oct. 2021.

ANITA MANASSAKORN received the Medical degree, in 1998. She completed the Residency Training in ophthalmology from Chiang Mai University, in 2003. She also completed a Clinical Research Fellowship in glaucoma from the University of California at Los Angeles, Los Angeles, and the University of Pittsburgh Medical Center, USA, in 2004 and 2005. She is currently a Faculty Member of the Glaucoma Unit, Department of Ophthalmology, Faculty of Medicine, Chulalongkorn University, and King Chulalongkorn Memorial Hospital. Her research interests include glaucoma imaging, artificial intelligence in glaucoma imaging, diagnosis, and management.

SUPATANA AUETHAVEKIAT received the B.Eng. degree in electrical engineering from Chulalongkorn University, Thailand, in 1996, and the M.Eng. and Ph.D. degrees in information and communication engineering from The University of Tokyo, Japan, in 1999 and 2002, respectively. She is currently a Faculty Member of the Department of Electrical Engineering, Chulalongkorn University. Her research interests include medical image processing and recognition, image segmentation, image classification, artificial intelligence and machine learning in images and videos, and data analytics.

VERA SA-ING received the bachelor's degree in computer engineering from the Suranaree University of Technology, in 2005, the master's degree in biomedical engineering from Mahidol University, in 2011, and the Doctor of Philosophy degree in electrical engineering from Chulalongkorn University, in 2017. He is currently a Faculty Member of the Department of Computer Science, Faculty of Science, Srinakharinwirot University. His research interests include biomedical imaging, image and video processing, artificial intelligence and machine learning in images and videos, robotic, and data analytics.

SUNEE CHANSANGPETCH received the M.D. degree (Hons.) from Chulalongkorn University, Bangkok, Thailand, in 2007, the B.P.H. degree in public health administration from Sukhothai Thammathirad University, Bangkok, in 2010, and the Clinical Science (Diploma) degree in ophthalmology from Chulalongkorn University, in 2012. She is currently a Board-Certified Ophthalmologist at King Chulalongkorn Memorial Hospital and works as a Faculty Member of the Department of Ophthalmology, Chulalongkorn University. She completed her Ophthalmology Residency and Glaucoma Fellowship at King Chulalongkorn Memorial Hospital, in 2012 and 2014, respectively. In 2018, she finished a Clinical Research Fellowship in glaucoma at the University of California at San Francisco, San Francisco, USA. Her research interests include ocular biomechanics, glaucoma imaging, and innovations in glaucoma diagnosis.

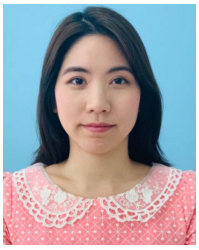

KITIYA RATANAWONGPHAIBUL received the Medical degree, in 2010. She completed Residency Training in ophthalmology from Chulalongkorn University, in 2016, where she also completed a Clinical Fellowship in glaucoma, in 2018. She also completed Postdoctoral Research Fellowship Program from Massachusetts Eye and Ear, Harvard medical School, USA, in 2019. She is currently a Faculty Member of the Glaucoma Unit, Department of Ophthalmology, Faculty of Medicine, Chulalongkorn University, and King Chulalongkorn Memorial Hospital. Her research interests include glaucoma investigations especially optic nerve imaging and visual field testing and new innovations in glaucoma management.

NOPPHAWAN URAMPHORN received the Medical degree, in 2010. She completed Residency Training in ophthalmology from Chulalongkorn University, in 2017. She also completed a Clinical Fellowship in glaucoma from King Chulalongkorn Memorial Hospital and the Thai Red Cross Society, in 2019. She is currently a Faculty Member of the Glaucoma Unit, Department of Ophthalmology, Faculty of Medicine Vajira Hospital, Navamindradhiraj University, Bangkok, Thailand. Her research interests include glaucoma imaging, artificial intelligence in glaucoma imaging, diagnosis, and management.

VISANEE TANTISEVI received the Medical degree (Hons.) from Chulalongkorn University, Bangkok, Thailand, and the Diploma degree in ophthalmology. She completed the Glaucoma Fellowship Training at King Chulalongkorn Memorial Hospital, Bangkok. Later, she received Certificate in Clinical Glaucoma Fellowship from The Royal Victorian Eye and Ear Hospital, Centre for Eye Research Australia (CERA), University of Melbourne, Australia. She holds a number of appointments, including an Associate Professor in ophthalmology; the Deputy Chairman of International Affairs; the Senior Instructor; the Residents' Advisory Board & Postgraduates Subcommittee; and the Chief and Consultant of Glaucoma Unit, Department of Ophthalmology, Faculty of Medicine, Chulalongkorn University. She is also a Glaucoma Consultant at the Queen Sirikit National Institute of Child Health and top-tier private hospital in Bangkok. She is also the Head of Public Relations and International Affairs for the Thai Glaucoma Society (ThGS), a Sub-Committee of Academic Affairs of The Royal college of Ophthalmologists of Thailand (RCOPT), and a Regular Invited Reviewer for several peer-reviewed journals in *Ophthalmology*. In addition, she is the current Deputy Secretary General of Asia Pacific Glaucoma Society. She also carries a lot of experiences in many fields. She has been doing, mentoring and participating in glaucoma diagnosis and therapeutic researches both locally and internationally. Under her advisement, one of the advisees was granted Prince Mahidol Youth Award, the renowned prestigious fund for medical student project. She has been entrusted to lead the organizing team of numerous national and international scientific meetings in which acclaimed at high success and being invited to speak and chair sessions in various national and international scientific conferences.